Competition between Hydrogen Bonding and Dispersion Interactions in the Indole···Pyridine Dimer and (Indole) 2 ···Pyridine Trimer Studied in a Supersonic Jet

ARTICLE *in* THE JOURNAL OF PHYSICAL CHEMISTRY A · JUNE 2011

Impact Factor: 2.69 · DOI: 10.1021/jp202658r · Source: PubMed

4 AUTHORS:

Sumit Kumar
Indian Institute of Science Education and Re…
9 PUBLICATIONS **72** CITATIONS
SEE PROFILE

Partha Biswas
Scottish Church College
12 PUBLICATIONS **66** CITATIONS
SEE PROFILE

Indu Kaul
Indian Institute of Science Education and Re…
4 PUBLICATIONS **27** CITATIONS
SEE PROFILE

Aloke Das
Indian Institute of Science Education and Re…
34 PUBLICATIONS **246** CITATIONS
SEE PROFILE

THE JOURNAL OF PHYSICAL CHEMISTRY A

ARTICLE

pubs.acs.org/JPCA

Competition between Hydrogen Bonding and Dispersion Interactions in the Indole···Pyridine Dimer and $(Indole)_2$···Pyridine Trimer Studied in a Supersonic Jet

Sumit Kumar, Partha Biswas, Indu Kaul, and Aloke Das*

Department of Chemistry, Indian Institute of Science Education and Research (IISER), 900, NCL Innovation Park, Dr. Homi Bhabha Road, Pune-411008, Maharashtra, India

Supporting Information

ABSTRACT: Structures of the indole···pyridine dimer and $(indole)_2$···pyridine trimer have been investigated in a supersonic jet using resonant two-photon ionization (R2PI) and IR-UV double resonance spectroscopic techniques combined with quantum chemistry calculations. R2PI spectra of the dimer and the trimer recorded by electronic excitation of the indole moiety show that the red-shift in the band origin of the dimer with respect to the 0_0^0 band of the monomer is larger compared to that of the trimer. The presence of only one conformer in the case of both the dimer and the trimer has been confirmed from IR-UV hole-burning spectroscopy. The structures of the dimer and the trimer have been determined from resonant ion dip infrared (RIDIR) spectra combined with ab initio as well as DFT/M05-2X and DFT/M06-2X calculations. It has been found that the dimer, observed in the experiment, has a V-shaped geometry stabilized by N−H···N and C−H···N hydrogen bonding interactions, as well as C−H···π and π···π dispersion interactions. The geometry of the trimer has been found to be a cyclic one stabilized by N−H···N, N−H···π, C−H···π, and C−H···N interactions. The most important finding of this current study is the observation of the mixed dimer and trimer, which are stabilized by hydrogen bonding as well as dispersion interactions.

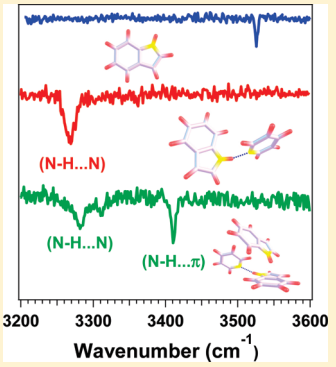

1. INTRODUCTION

Hydrogen bonding, as well as π···π stacking, and nonconventional hydrogen bonding such as N−H···π and C−H···π interactions play a significant role in governing the specific functional structures of important biomolecules such as proteins and nucleic acids.[1−3] Crystal engineering, supramolecular chemistry, self-assembly, molecular recognition, and DNA intercalation also deal with subtle balance among these noncovalent interactions.[4−12] The origins of the hydrogen bonding and stacking or π-hydrogen bonding interactions are entirely different. The hydrogen bonding one arises from electrostatic interaction, while dispersion forces dominate the π···π stacking and π-hydrogen bonding interactions. Though hydrogen bonding interaction could be determined quite precisely by both experiment and theory, accurate determination of dispersion interaction is extremely challenging.

Gas phase laser spectroscopy in a supersonic jet offers an ideal means to study the intermolecular forces present in noncovalently bonded aromatic dimers and higher clusters. Experimental results available in the isolated gas phase are also very much desirable to compare with the data available from very high level quantum chemistry calculations. Up to this date, the most extensively studied aromatic dimer using numerous experimental as well as theoretical investigations is the benzene dimer.[13−29] The binding energy difference between parallel-displaced π-stacked and T-shaped benzene dimer is very small (about 0.1 kcal/mol) according to the highly accurate quantum chemistry calculation at CCSD(T)/CBS level.[27] But gas phase supersonic jet studies show the presence of only the T-shaped dimer of benzene stabilized due to C−H···π interaction.[13−18] These benchmark studies on benzene dimer demonstrate that C−H···π interaction is slightly stronger than the π···π interaction. On the other hand, the benzene···NH_3 complex has been studied quite extensively as a model for NH···π interaction employing both experimental as well theoretical methods.[30,31] NH···π bound slanted T-shaped geometry has been confirmed in the case of the pyrrole dimer by a few groups.[32,33] Leutwyler and coworkers have reported quite strong NH···π interaction in the case of the 2-pyridone···benzene dimer where the N−H stretching frequency is red-shifted by 56 cm^{-1}.[34] Indole··· benzene dimer has been studied by mass analyzed threshold ionization experiment as well as quantum chemistry calculations.[35−37] It has been found from CCSD(T)/CBS level of calculation that NH···π bound T-shaped geometry of the dimer is more stable than the parallel-displaced π-stacked one by about 1.1 kcal/mol.[37] Thus, the experimentally observed dimer is assigned to have NH···π bound T-shaped structure. It can be concluded from these studies that NH···π interaction is also stronger than the

Received: December 12, 2010
Revised: May 11, 2011
Published: June 02, 2011

$\pi\cdots\pi$ interaction present in aromatic dimers. Given that there is a competition among classical hydrogen bonding, unconventional π-hydrogen bonding, and stacking interactions in aromatic clusters, it is quite challenging to study the structures of the molecular systems, which are stabilized due to electrostatic as well as dispersion interactions.

The primary aim of the present spectroscopic investigation is to study the special class of mixed complexes where the geometries of the complexes are determined by the subtle balance between conventional hydrogen bonding as well as dispersion interactions. A study of this kind of mixed complexes in the literature is very scarce. The theoretical determination of the geometries of the mixed complexes is extremely challenging as the conventional DFT functional does not include dispersion interaction, and MP2 level calculations overestimate the dispersion interaction. In general, the mixed complexes, reported in the S22 database, are defined as the complexes that contain a mixture of electrostatic and dispersion interactions.[38] Among the seven mixed complexes reported in the S22 database, only the phenol dimer falls in the category of the special class of mixed complex. It has been confirmed from various experimental and theoretical studies that the geometry of the phenol dimer is dictated by strong hydrogen bonding interaction as well as CH$\cdots\pi$ and $\pi\cdots\pi$ dispersion interactions.[39−45]

In this study, we have investigated the structures of the indole$\cdots$pyridine dimer and (indole)$_2\cdots$pyridine trimer in the supersonic jet by employing resonant two photon ionization (R2PI), infrared-ultraviolet (IR-UV) double resonance spectroscopic techniques and quantum chemistry calculations. The motivation behind studying the complexes of indole and pyridine is as follows. Indole$\cdots$pyridine dimer and (indole)$_2\cdots$pyridine trimer are a special class of mixed complexes like phenol dimer, where the unique geometries of the complexes are determined by both hydrogen bonding and dispersion interactions. Moreover, the spectroscopic study of complexes of indole and pyridine has specific biological relevance as it mimics protein−enzyme interaction.[46,47] Essentially this current investigation models the interaction of the side chain of tryptophan with pyridine coenzymes. Up to this date, there is no report in the literature for the experimental study of complexes of indole and pyridine, although there is a computational study that focuses on the binding energies of only π-stacked conformers of the mixed dimer.[46] The most significant finding of the present investigation is the observation of the indole$\cdots$pyridine dimer and (indole)$_2\cdots$pyridine trimer, where the geometry of the dimer is stabilized by N−H$\cdots$N and C−H$\cdots$N hydrogen bonding as well as CH$\cdots\pi$ and $\pi\cdots\pi$ dispersion interactions, whereas the trimer has a cyclic geometry governed by N−H$\cdots$N and C−H$\cdots$N hydrogen bonding as well as NH$\cdots\pi$ and CH$\cdots\pi$ dispersion interactions.

2. METHODS

2.1. Experimental Section. A home-built jet-cooled resonantly enhanced multiphoton ionization (REMPI) time-of-flight mass spectrometer (TOFMS) has been used in this study. The setup consisted of two differentially pumped vacuum chambers connected through a skimmer (Beam Dynamics Inc.) of 2 mm diameter. The pulsed valve with an orifice diameter of 0.5 mm (General valve, series 9, rep. rate 10 Hz) was incorporated in the bigger chamber (expansion chamber) pumped by a 10 in. diffstack diffusion pump (OD250, Hind Hivac). The nozzle to skimmer distance was kept fixed at about 25 mm. A two-stage ion source of Wiley−McLaren design[48] with a 1 m linear time-of-flight tube (Jordan TOF Products) was housed in the smaller chamber (ionization chamber) pumped by a 4.5 in. diffstack diffusion pump (OD114, Hind Hivac).

To synthesize the complexes of indole and pyridine in a supersonic jet, the following procedure was followed. Indole (Sigma-Aldrich) was put in a stainless steel sample holder placed immediately behind the pulsed valve and heated at about 80 °C. The argon buffer gas, at a pressure of about 40 psig, was bubbled through pyridine (Sigma-Aldrich), taken in a stainless steel sample container maintained at 0 °C and kept outside the vacuum chamber. Pyridine vapor seeded in the buffer gas was mixed with indole vapor and expanded into vacuum through the pulsed nozzle.

Typical operating pressures in the expansion and ionization chambers were 5×10^{-6} and 6×10^{-7} Torr, respectively. The collimated molecular beam was ionized using the one-color resonant two-photon ionization (1C-R2PI) technique by frequency doubled output of a tunable dye laser (ND6000, Continuum) pumped by the second harmonic of a Nd:YAG laser (nanosecond, 10 Hz, Surelite II-10, Continuum). The resolution of the dye laser is about 0.08 cm^{-1}. Typical UV pulse energy used for ionization was about 0.4−0.5 mJ. The ions were mass analyzed in the time-of-flight mass spectrometer and detected by an 18 mm diameter dual MCP detector (Jordan TOF Products) placed at the end of the time-of-flight tube. The detector was housed in a small chamber, which is pumped by a 70 L/s turbomolecular pump (Turbo-V81, Varian). The ion signal from the detector was amplified using a preamplifier (SRS, Model SR445A) and sent to a digital oscilloscope (Tektronix, 350 MHz, DPO 4034) interfaced to a PC via a USB port. Both data acquisition and laser control were performed using home-built LabView (National Instruments, 8.6 version) based programs.

IR spectra of the complexes of indole and pyridine were measured using resonant ion dip infrared spectroscopy (RIDIRS). In this technique, two counter-propagating IR and UV laser beams were spatially overlapped and intersected the molecular beam at right angle. Typical pulse energy of IR laser beam used was about 5−6 mJ and it was focused using a CaF_2 lens of focal length 185 cm, whereas the UV laser beam used was unfocused and the typical energy was about 0.4 mJ. IR laser, which was fired about 100 ns prior to the UV laser, was scanned through the vibrational transitions in the ground electronic state, while the UV laser was fixed to a particular transition in the R2PI spectrum of the dimer. Thus, IR spectra were obtained as depletion of the ion signal, whenever the IR laser frequency was matching with any vibrational transition of the complexes in the ground electronic state. Further IR-UV hole-burning experiment was performed to discriminate the transitions in the R2PI spectrum, which belong to different conformers. This technique is just opposite to RIDIRS. Here the IR laser was kept fixed at a particular vibrational frequency of a conformer and the UV laser, which was fired after 50−100 ns from the IR laser was scanned through the R2PI spectral region. As the IR laser would burn the population of a specific conformer through vibrational excitation, the UV excitation peaks of that conformer would show reduced intensity compared to those in the R2PI spectrum. On the other hand, the intensity of the UV excitation peaks of the other conformers in the R2PI spectrum would be unaltered even in the presence of the IR beam. The tunable IR laser was a KTA based OPO (Laser Vision) pumped by an unseeded Nd:YAG laser (ns, 10 Hz, Surelite II-10). Typical resolution of the IR laser used in the

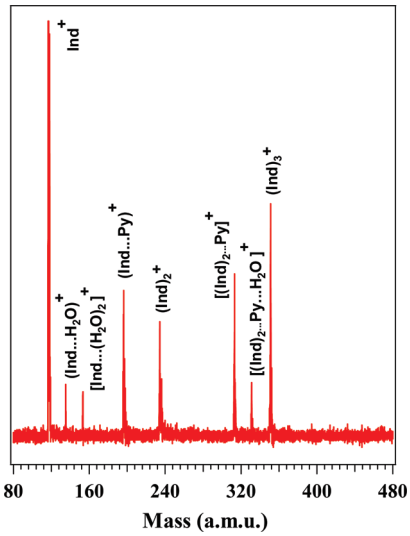

Figure 1. TOF mass spectrum of indole in presence of pyridine recorded at laser frequency of 35191 cm^{-1}, which corresponds to one of the electronic transition bands of the (indole)$_2$···pyridine complex. Ind and Py stand for indole and pyridine, respectively.

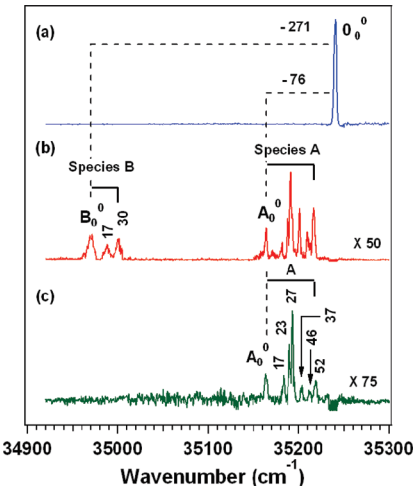

Figure 2. One-color R2PI spectra recorded in (a) indole, (b) indole···pyridine dimer, and (c) (indole)$_2$···pyridine trimer mass channels. R2PI signals of the dimer and the trimer are very weak compared to that of the monomer. Thus, the dimer and the trimer spectra are magnified by 50 and 75 times, respectively.

experiment is about 2−3 cm^{-1}. Temporal synchronization among the pulsed valve and various lasers is controlled by using a digital delay generator (BNC, Model 575).

2.2. Computational Section. Ground state geometry optimizations of all possible conformers of indole···pyridine dimer were performed initially at the MP2/6-31+G* level of theory. Four low energy conformers of the dimer obtained at MP2/6-31+G* level were further optimized at DFT/M05-2X, DFT/M06-2X, and MP2 levels using cc-pVDZ and aug-cc-pVDZ basis sets. Structures of (indole)$_2$···pyridine trimer were optimized at DFT/M05-2X and DFT/M06-2X levels. Harmonic vibrational frequency calculations of various conformers of the dimer and the trimer at different levels of theory were performed to confirm that the optimized geometries were corresponding to local minima as well as to compare with the observed IR frequencies of the complexes present in the experiment. For DFT calculations, an "ultrafine" numerical integration grid was used to obtain reliable results for complexes with noncovalent interactions. The binding energies of various conformers of the dimer and the trimer were corrected for basis set superposition error (BSSE) and zero point vibrational energy. BSSE correction was done using the counterpoise method given by Boys and Bernadi.[49] Energy decomposition analysis of the intermolecular interactions of the dimer and the trimer was done using a localized molecular orbital (LMO) method available in GAMESS, U.S.A.[50] MP2 and DFT/M05-2X calculations were performed using the Gaussian 03 program package,[51] while NWChem software[52] was used for DFT/M06-2X calculations.

3. RESULTS AND DISCUSSION

3.1. Time of Flight (TOF) Mass Spectrum. Figure 1 shows TOF mass spectrum of complexes of indole and pyridine in argon buffer gas recorded at a laser frequency of 35191 cm^{-1}, which corresponds to one of the electronic transition bands of the (indole)$_2$···pyridine complex. The mass peak observed at 196 amu is due to the indole···pyridine dimer, whereas the 313 amu mass peak is designated as the (indole)$_2$···pyridine trimer. Higher clusters of indole, that is, (indole)$_2$ and (indole)$_3$, are also observed at 234 and 351 amu, respectively. Water clusters of indole, that is, indole···$(H_2O)_1$ and indole···$(H_2O)_2$, as well as (indole)$_2$···pyridine···(H_2O), are also formed in the experiment due to the presence of water as an impurity in the sample and the buffer gas.

3.2. Resonant 2-Photon Ionization (R2PI) Spectra. One-color R2PI spectra recorded in indole···pyridine dimer and (indole)$_2$···pyridine trimer mass channels are shown in Figure 2b and c, respectively. One-color R2PI spectrum of indole in the absence of pyridine is also shown in Figure 2a to compare with dimer and trimer R2PI spectra. The origin band (0_0^0) for the $S_0 \rightarrow S_1$ electronic transition of indole appears at 35240 cm^{-1}.[53] The R2PI spectra of complexes of indole and pyridine are measured by electronic excitation of the indole moiety. R2PI signals of the dimer and the trimer are very weak, and thus, the dimer and trimer R2PI spectra are magnified by 50 and 75 times, respectively, to show in the same graph with the spectrum of the indole monomer. The R2PI spectrum in the indole···pyridine dimer mass channel shows two different sets of bands originated due to electronic transitions of two different species designated as A and B. When the R2PI spectrum is recorded in the (indole)$_2$···pyridine trimer mass channel, all the peaks assigned as A in the dimer channel also appear in the trimer mass channel. This confirms that the peaks assigned as A do not belong to the indole···pyridine dimer, rather it seems that these peaks are originated due to electronic transition of (indole)$_2$···pyridine trimer. These peaks appear in the R2PI spectrum recorded in the dimer mass channel due to efficient fragmentation of the (indole)$_2$···pyridine trimer in the indole···pyridine dimer mass channel. R2PI spectrum in the mass channel of indole in presence of pyridine is also recorded and this indicates the fragmentation of A and B complexes into indole monomer channel as well. But the spectrum in the indole mass channel is complicated due to overlapping of the transitions arise from the fragmentation of other higher clusters of indole. Thus, the R2PI spectrum in the indole mass channel in presence of pyridine is not presented here. To avoid the fragmentation of the clusters, generally two-color R2PI scheme is used by fixing the ionization

Table 1. Tentative Assignment of the Observed Intermolecular Vibrations of (Indole)$_2$···Pyridine Trimer

frequencies (cm^{-1})	assignment
17	β
23	δ
27	θ
37	$2\beta/\beta+\delta$
46	$2\delta/\beta+\theta$
52	$2\theta/3\beta/\theta+\delta$

laser frequency just above the ionization threshold. We have tried two-color R2PI of complexes of indole and pyridine, but it was not successful, probably due to very fast deactivation of the S_1 state. We have also recorded R2PI spectrum in the (indole)$_2$···pyridine···H_2O channel, which is observed in the mass spectrum depicted in Figure 1. It is possible that (indole)$_2$···pyridine···H_2O complex may fragment to (indole)$_2$···pyridine trimer and indole···pyridine dimer mass channels. But the R2PI spectrum recorded in (indole)$_2$···pyridine···H_2O mass channel (see Figure S1 in Supporting Information) does not show any peak in the region of the R2PI spectrum of either species A or B. From the R2PI spectra recorded in various observed mass channels, it can be concluded that the species A is (indole)$_2$···pyridine trimer, which is confirmed in the following sections through IR-UV double resonance spectroscopy and quantum chemistry calculations.

Figure 2 shows that the origin band (B_0^0) of the indole···pyridine dimer is red-shifted from the 0_0^0 band of the indole monomer by 271 cm^{-1}. The transitions marked at B_0^0+17, and B_0^0+30 cm^{-1} are assigned as intermolecular vibrations of the mixed dimer. In the case of (indole)$_2$···pyridine trimer, the origin band (A_0^0) is red-shifted from the 0_0^0 band of indole monomer by 76 cm^{-1}. The low frequency vibronic features built off A_0^0 band are assigned as intermolecular vibrations of the trimer. The assignment is confirmed in the following section through RIDIR and IR-UV double resonance spectroscopy. Intermolecular vibrations of the trimer observed in the R2PI spectrum shown in Figure 2c are listed in Table 1 and a tentative assignment of those vibrations is also provided there. All of the vibronic features in the spectrum can be tentatively explained as overtone and combination bands of mostly three intermolecular modes of 17 (β), 23 (δ), and 27 (θ) cm^{-1}. Proper assignment of the low frequency vibrations in the R2PI spectrum can be done only by performing excited state frequency calculation of the trimer, which is not possible using our available computational resources. But we have performed the frequency calculation of the trimer in the ground electronic state and 12 intermolecular vibrational frequencies of the most stable conformer of the trimer are listed in Table S1. We are aware that the calculated frequencies in the excited state will be different and thus the observed excited state intermolecular vibrational frequencies are not compared with the calculated frequencies in the ground electronic state.

One characteristic feature of the R2PI spectrum of the trimer is that the 0_0^0 band (A_0^0) is weaker in intensity compared to a few of the low frequency intermolecular vibrations built on it. This indicates that the ground state equilibrium geometry of the trimer is changed significantly upon electronic excitation to the S_1 state, and the geometry change of the trimer along 27 cm^{-1} mode is the maximum upon electronic excitation. But the excitation spectrum does not show extensive Franck−Condon progressions, although multiple intermolecular modes are clearly observed. Absence of further vibrational progressions could be due to the following reason. Actually, few low frequency vibrations beyond 52 cm^{-1} are overlapping with the 0_0^0 band position of the indole monomer. The UV laser is blocked in the region of origin band of bare indole to avoid detector saturation due to a very strong ion signal of the monomer. This leads to a small dip in the origin band position of indole in the R2PI spectra of the complexes shown in Figure 2.

It is interesting to note that the red-shift in the band origin of the (indole)$_2$···pyridine trimer with respect to the 0_0^0 band of indole is much less compared to that of the indole···pyridine dimer. This indicates that the stabilization of the dimer in comparison to the trimer is more in the S_1 state. A similar kind of trend is also observed in the case of the phenol dimer and trimer.[40] The red-shifts in the band origins of the phenol dimer and trimer are 304 and 146 cm^{-1}, respectively, with respect to the 0_0^0 band of phenol monomer. It is also worthy to compare the line widths of the transitions in indole···pyridine dimer, (indole)$_2$···pyridine trimer, and bare indole, which can shed light on the photophysics of the complexed indole in the excited electronic state. The line width of the 0_0^0 band of the indole monomer is about 3 cm^{-1}, whereas the line widths of resonances in the indole···pyridine dimer and (indole)$_2$···pyridine trimer are about 6.5 and 2.5 cm^{-1}, respectively. The line width of transitions and the lifetime of the molecules in the excited state are inversely proportional to each other. Thus, the dimer has a much shorter lifetime in the S_1 state compared to that of bare indole as well as the trimer. This observation is nicely supported by a few investigations reported in the literature. Sobolewski and Domcke have studied the photophysics of the hydrogen-bonded dimer of the indole and pyridine by calculating the potential energy profiles of the ground and lowest excited electronic states of the complex as a function of the NH stretching coordinate.[54] They have found that there is ultrafast internal conversion between the S_1 (^1L_b) and S_0 states of the hydrogen-bonded dimer through the ^{1}CT (charge transfer) state via conical intersection. Hager and Wallace have reported that fluorescence of indole is completely quenched in the presence of pyridine in the solution phase and supersonic jet studies.[55] They have explained that the deactivation of the S_1 state is due to either fast internal conversion to the S_0 state or intersystem crossing to the triplet manifold. The fast deactivation of the S_1 state of the dimer can also be explained in terms of efficient energy transfer from the indole moiety to pyridine after electronic excitation of indole as $S_0 \rightarrow S_1$ energies of indole and pyridine are close to each other. The excitation energies for 0_0^0 transitions to the S_1 (^1L_b) state of indole and S_1 ($^1B_1$) state of pyridine are 35240 and 34771 cm^{-1}, respectively.[56]

3.3. RIDIR Spectra. To determine the structures of the indole···pyridine dimer and the (indole)$_2$···pyridine trimer observed in the experiment, IR spectra in the NH stretching frequency region have been recorded by probing several transitions in the R2PI spectrum of the dimer and the trimer. RIDIR spectrum presented in Figure 3a shows the appearance of NH stretching fundamental of indole monomer at 3526 cm^{-1}, which agrees very well with the previous report.[57] Figure 3b shows RIDIR spectrum obtained by probing B_0^0+30 cm^{-1} band of indole···pyridine dimer. The spectrum shows a single band at 3269 cm^{-1} and this is assigned to the NH stretching vibration of the dimer. The NH stretching vibration of the dimer is red-shifted by 257 cm^{-1} from that of indole monomer. Theoretical

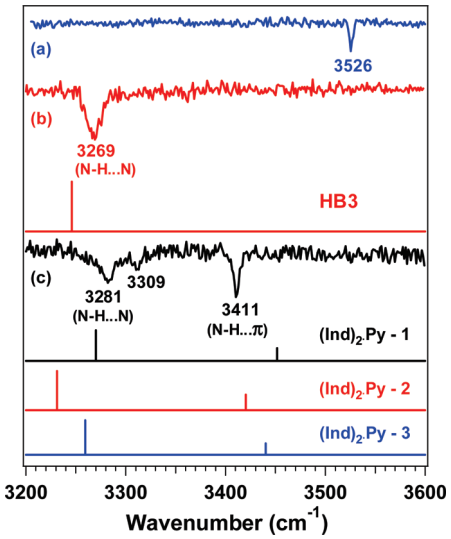

Figure 3. RIDIR spectra by probing the (a) 0_0^0 band of indole, (b) $B_0^0 + 30\ cm^{-1}$ band of indole···pyridine dimer, and (c) $A_0^0 + 27\ cm^{-1}$ band of $(indole)_2$···pyridine trimer in the N−H stretching region. Theoretical IR spectra for V-shaped (HB3) conformer of indole···pyridine dimer, and three conformers of $(indole)_2$···pyridine trimer are provided in (b) and (c), respectively.

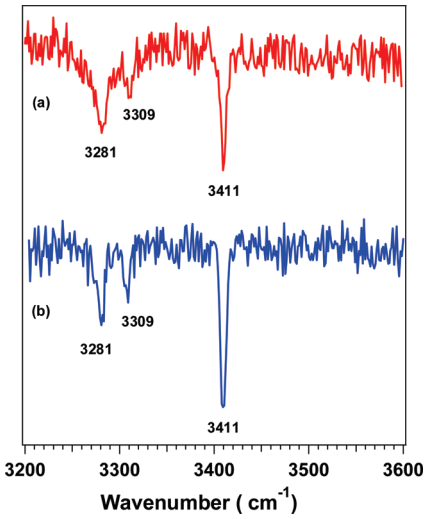

Figure 4. RIDIR spectra in the N−H stretching region by probing $A_0^0 + 27\ cm^{-1}$ electronic band obtained in (a) $(indole)_2$···pyridine trimer and (b) indole···pyridine dimer mass channels.

IR spectrum of the hydrogen bonded (N−H···N) dimer shown with Figure 3b matches very well with the experimental spectrum. Thus, the dimer has a hydrogen bonded structure with N−H···N interaction. RIDIR spectrum by probing $A_0^0 + 27\ cm^{-1}$ transition of $(indole)_2$···pyridine trimer is depicted in Figure 3c. The spectrum shows a strong band at 3411 cm^{-1} and two other bands at 3281 and 3309 cm^{-1}. Theoretical IR spectra of three probable structures of $(indole)_2$···pyridine trimer are shown with Figure 3c. IR spectra of all three structures of the trimer reproduce two experimental peaks at 3281 and 3411 cm^{-1} with some variation. Thus, it is assigned that the 3281 cm^{-1} peak is originating from the hydrogen-bonded (N−H···N) N−H stretch, whereas the 3411 cm^{-1} peak is due to π-hydrogen-bonded (N−H···π) N−H stretch in the trimer. The IR peak at 3309 cm^{-1} is assigned to the intermolecular vibration (27 cm^{-1}) of the trimer built off the hydrogen-bonded N−H stretching (N−H···N) vibration at 3281 cm^{-1}. The 27 cm^{-1} vibration is the most intense intermolecular mode observed in the electronic spectrum of the trimer. Observation of combination bands involving hydrogen-bonded N−H or O−H stretch and low frequency intermolecular vibrations of the complexes are extensively reported in the literature.[57−60] It is also interesting to point out that the 3309 cm^{-1} band could not be due to the C−H stretching modes of either indole or pyridine moieties of $(indole)_2$···pyridine trimer. IR spectra of jet-cooled indole as well as 2-fluoropyridine in the C−H stretching region have been reported in the literature.[57,61] C−H stretching frequencies of indole and 2-fluoropyridine appear in the range of 3000−3200 and 3000−3100 cm^{-1}, respectively. Gas phase FTIR spectrum of pyridine is also reported in the literature, and this shows C−H stretching frequencies in the 3000−3100 cm^{-1} range.[62]

The most probable structure of the observed trimer is further determined from the comparison of binding energies and relative energies of the three structures of the trimer and this has been discussed in the theoretical section. Figure 4 shows RIDIR spectra by probing $A_0^0 + 27\ cm^{-1}$ electronic transition obtained in both $(indole)_2$···pyridine trimer as well as indole···pyridine dimer mass channels. Identical IR spectra have been obtained in both of the cases and this confirms that species A is trimer only.

The magnitudes of the red-shift in the X-H stretching frequency as well as width of the peak measure the strength of the hydrogen bond. It is interesting to note that the red-shift in the hydrogen-bonded (N−H···N) N−H stretching frequency in the trimer (245 cm^{-1}) is very similar to that in the dimer (257 cm^{-1}). The π-hydrogen bonded N−H stretching frequency in the trimer is red-shifted by 115 cm^{-1}. The fwhm of N−H···N bound N−H stretching bands for indole···pyridine dimer and $(indole)_2$···pyridine trimer is about 20 and 12 cm^{-1} respectively, whereas the width of the π-hydrogen bound N−H stretching band is about 8 cm^{-1}. For comparison, we can refer to the fwhm of the free NH stretching band of indole monomer, which is about 4 cm^{-1}. Overall results indicate that N−H···N hydrogen bonding interaction in the dimer is slightly stronger than that in the trimer. As expected, NH···π hydrogen bonding interaction in the trimer is weaker than N−H···N hydrogen bonding interaction observed in the dimer as well as the trimer.

Interestingly, identical IR spectra were obtained by probing most of the electronic transitions of the trimer. Figure 5 displays IR spectra by probing A_0^0, $A_0^0 + 27$, and $A_0^0 + 37\ cm^{-1}$ transitions of $(indole)_2$···pyridine trimer observed in the R2PI spectrum recorded in the dimer mass channel and these show similar IR spectral features. This confirms that the lowest energy electronic transition for species A marked as A_0^0 is the origin band of the trimer and all of the higher energy transitions built off A_0^0 are only due to intermolecular vibrations of only one conformer of the trimer. Identical IR spectra were also obtained by probing all the three bands in the R2PI spectrum of the dimer, that is, B_0^0, $B_0^0 + 17$, and $B_0^0 + 30\ cm^{-1}$ (see Figure S2 in the Supporting Information). This demonstrates that all these three transitions belong to only one conformer of the dimer.

3.4. IR-UV Hole-Burning Spectra. IR-UV hole-burning spectra obtained by probing the vibrational bands of the dimer and the trimer observed in the RIDIR spectra have been shown in

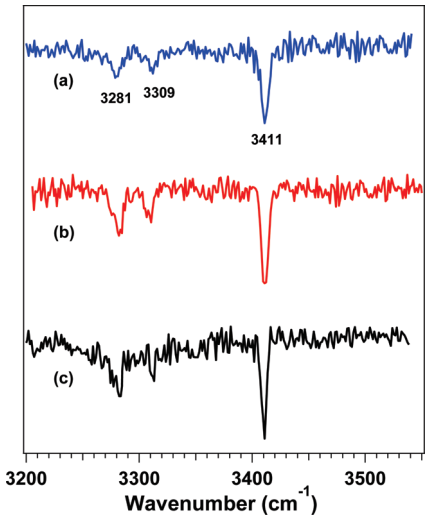

Figure 5. RIDIR spectra in the N−H stretching region by probing (a) A_0^0 band, (b) $A_0^0 + 27$ cm^{-1} band, and (c) $A_0^0 + 37$ cm^{-1} band of (indole)$_2$···pyridine trimer obtained in the indole···pyridine dimer mass channel.

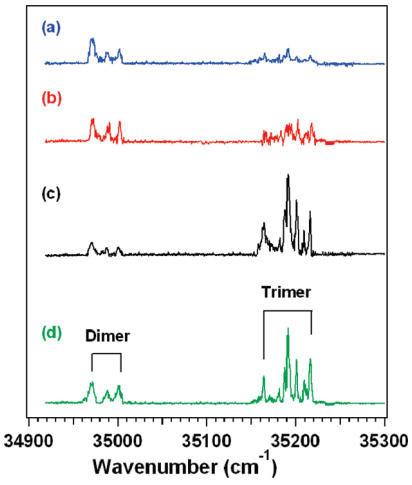

Figure 6. IR-UV hole-burning spectra recorded in the indole···pyridine dimer mass channel by pumping the vibrational bands at (a) 3411 cm^{-1}, (b) 3281 cm^{-1}, and (c) at 3269 cm^{-1}. (d) R2PI spectrum in the indole···pyridine dimer mass channel.

Figure 6. Figure 6d shows the R2PI spectrum of the complexes of indole and pyridine in the dimer mass channel, which is identical to the spectrum already shown in Figure 2b. The hole-burning spectrum by exciting the π-bound N−H stretching vibrational band of the trimer at 3411 cm^{-1} is provided in Figure 6a. The spectrum shows the dip in ion signals for all the electronic transitions designated for the trimer while the bands assigned due to the electronic transitions for the dimer appeared with similar intensity as observed in the R2PI spectrum shown in Figure 6d. This clearly demonstrates that all the bands grouped as A belong to same conformer of the trimer. When the σ-bound N−H stretching vibrational band of the trimer at 3281 cm^{-1} is excited, similar hole-burning spectrum like the one in Figure 6a is observed and the spectrum is shown in Figure 6b. IR-UV hole-burning spectrum by probing the vibrational band of the trimer at 3309 cm^{-1} is also recorded and has been shown in Figure S3 (see Supporting Information). The hole-burning spectrum at 3309 cm^{-1} is also similar like the spectra shown in Figure 6a,b. Figure 6c shows the hole-burning spectrum by exciting the N−H stretching vibrational band of the dimer at 3269 cm^{-1}. The spectrum shows the dip in the ion signals only for the bands assigned due to the electronic transitions for the dimer while the transitions designated for the trimer appeared with similar intensity as observed in Figure 6d. Thus, considering IR-UV hole-burning spectra in Figure 6a−c, it is confirmed that each dimer and trimer shows only one conformer in the experiment.

3.5. Theoretical Results. *3.5.1. Structures of Indole···Pyridine Dimer.* Several isomeric structures of indole···pyridine dimer with different possible orientations of the two monomer units are shown in Figure 7. These structures have been used as starting geometries for optimization. To construct the starting geometries for the dimer, we have followed the similar scheme adopted by Sickle et al. and Geng et al. for the indole···benzene dimer.[63,64] In our case, geometric isomers of the indole··· pyrdine dimer have been classified mainly into three different categories, namely, hydrogen-bonded (HB), T-shaped (T), and parallel-displaced (PD). In both HB1 and HB2 structures, there is a strong hydrogen bond between the indole NH and the nitrogen atom of pyridine. But, in the case of HB1, indole and pyridine are oriented in a perpendicular fashion to each other through a N−H···N hydrogen bond, while indole and pyridine are in the same plane in HB2. T1, T2, and T3 structures consist of CH···π hydrogen bonding with a phenyl group, fused C=C bond, and the pyrrole group of indole, respectively, while CH···π hydrogen bonding with both phenyl and pyrrole groups are present in the T4 structure. The T5 structure is characterized by NH···π hydrogen bonding, where the NH group of indole makes hydrogen bonding with the π-cloud of pyridine. Anti-PD1, anti-PD2, and anti-PD3 structures have anti-parallel-displaced geometry with pyridine placed in the stacked fashion over the phenyl ring, pyrrole ring, and fused C=C bond of indole, respectively. As the indole N−H group and pyridine nitrogen atom are oriented on the opposite side for PD1, PD2, and PD3 structures, those are called anti-parallel-displaced stacked. The syn-PD4 structure is obtained by placing pyridine over the indole ring in a stacking orientation, where the indole N−H and pyridine nitrogen atom are facing the same side.

It is obvious that dispersion interaction has significant contribution in stabilization of most of the isomeric structures of the indole···pyridine dimer shown in Figure 7. Thus, initial geometry optimization of all 11 probable structures was done at the MP2/6-31+G* level. The results of this initial geometry optimization are only described below in the text and both input and output structures at MP2/6-31+G* have been provided in Figure S4 in the Supporting Information. Optimization of HB1 structure led to V-shaped hydrogen-bonded structure HB3, which has been shown in Figure 8b. HB2 structure was also transformed into V-shaped HB3 structure after optimization, which is due to steric repulsion of adjacent hydrogen atoms of indole and pyridine in the planar HB2 geometry. T1, T2, T3, and T4 structures were converted into syn-PD4 structure after optimization. Optimization of anti-PD1, anti-PD2, and anti-PD3 structures led to anti-PD3 structure. NH···π bound T5 structure gave one imaginary frequency at MP2/6-31+G* level of calculation. Thus, four isomeric structures of the dimer out of 11 probable structures optimized further at various levels of theory are HB3, anti-PD3, syn-PD4, and T5 (NH···π). Figure 8a shows atom-numbering scheme used in geometry

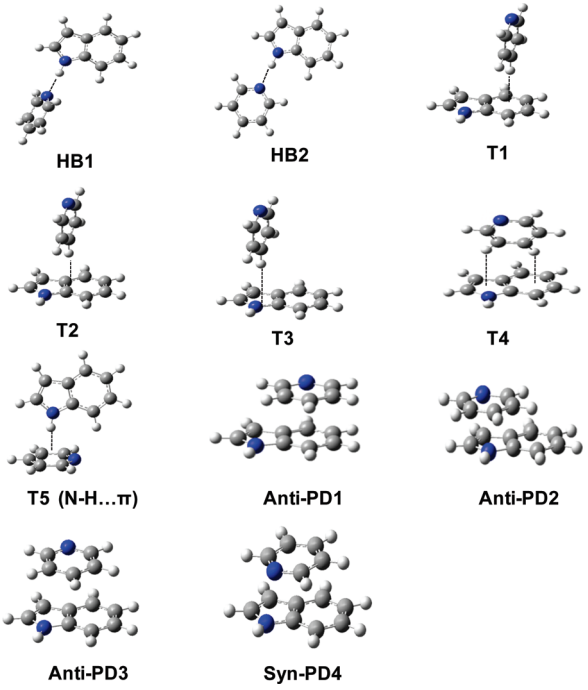

Figure 7. Structures of possible conformers for the indole···pyridine dimer. These structures are used as initial geometries for optimization.

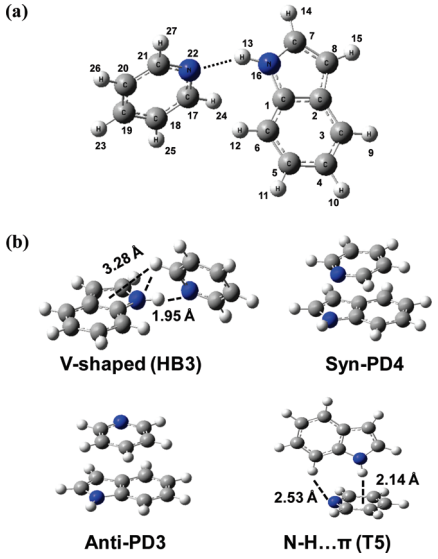

Figure 8. (a) Atom-numbering scheme in indole···pyridine dimer, and (b) MP2/aug-cc-pVDZ optimized structures of four conformers of indole···pyridine dimer.

optimization of indole···pyridine dimer and this numbering scheme is used to compare important calculated geometric parameters of various conformers of the dimer. Figure 8b shows the structures of the four conformers of the dimer optimized at MP2/aug-cc-pVDZ level. As MP2 level of calculation overestimates the dispersion interaction, DFT/M05-2X and DFT/M06-2X levels of calculations were also done using various basis sets to obtain reliable binding energies of these conformers of the dimer. It is well-known that the traditional DFT functional like B3LYP does not include dispersion interaction. Thus, the DFT/B3LYP method very often neither accurately computes the interaction energies of dispersion-dominated complexes nor describes their structures properly. But, recently developed meta-density functionals M05-2X and M06-2X by Zhao and Truhlar provide much improved results for noncovalently bonded complexes having dispersion interaction.[65] Sponer et al. have demonstrated that the mean average error of the interaction energies of stacked complexes of nucleic acid bases computed at the DFT/M05-2X level is even smaller than that computed at the MP2/CBS level.[66]

The BSSE and zero point energy (ZPE) corrected binding energies for all the four conformers of the dimer calculated at various levels of theory are presented in Table 2. Comparison of binding energies of the conformers at various levels of theory clearly shows that the most stable conformer is the V-shaped (HB3) one. ZPE-corrected relative energies of the four conformers of the dimer are also calculated and provided in Table S2 (see Supporting Information). The result shows that the V-shaped HB3 conformer of the dimer is the global minimum. BSSE corrected binding energy of the syn-PD4 conformer at the MP2/aug-cc-pVDZ level is very close to that of the V-shaped conformer (HB3), which clearly demonstrates the overestimation of the dispersion interaction of the stacked conformer at the MP2 level. ZPE correction of the binding energies of the four conformers of the dimer was not done at MP2/aVDZ and M06-2X/aVDZ levels as frequency calculations of the dimer at those levels are very expensive. Very recently, Sanders has calculated the binding energies of only π-stacked conformers of the indole···pyridine dimer at MP2/aug-cc-pVDZ//MP2-cc-pVDZ level of theory.[46] It is interesting to compare our computed results with these reported values. The binding energies of the syn-parallel-displaced π-stacked (syn-PD4) and anti-parallel-displaced π-stacked (anti-PD3) conformers reported by Sanders are −8.75 and −7.03 kcal/mol, respectively, whereas the respective values calculated by us at MP2/aug-cc-pVDZ are −8.39 and −6.67 kcal/mol. It is obvious that our results agree very well with the reported one.

Few important geometric parameters of the four conformers of the dimer calculated at MP2/aug-cc-pVDZ level of theory are listed in Table 3. Frequencies of the four conformers calculated at the MP2/cc-pVDZ level of theory are also provided in the same table. Theoretical N−H stretching frequency of indole monomer calculated at MP2/cc-pVDZ level is 3686 cm^{-1}, while experimental N−H stretching frequency of indole monomer is 3526 cm^{-1}. Thus, a scaling factor of 0.9566 is used to correct the theoretical N−H stretching frequencies of various conformers of the dimer. The most stable V-shaped conformer (HB3) possesses a strong intermolecular N−H···N hydrogen bond with H···N distance ($d_{H\cdots N}$) of 1.95 Å and N···N distance ($d_{N\cdots N}$) of 2.88 Å. Drastic increase in the N−H bond length (Δr_{N-H} = 0.015 Å) of indole upon formation of dimer with pyridine indicates the formation of a strong hydrogen bond in the V-shaped conformer. Though the geometry of this conformer is characterized by strong hydrogen bonding interaction, this is stabilized by additional dispersive interactions through weak C−H···π hydrogen bonding and displaced π···π interactions. If we carefully notice, weak C−H···N hydrogen bonding interaction is also present in the HB3 structure. The C−H···N hydrogen bonding distance in this structure is 2.72 Å. The presence of C−H···N interaction in the HB3 structure is also indicated by a little increase in the $^{17}C-H^{24}$ bond length of the pyridine ring compared to the other C−H bonds. $^{17}C-H^{24}$ bond length of the pyridine ring is 1.095 Å, whereas the length of

Table 2. BSSE and ZPE Corrected Binding Energies (kcal/mol) of Four Conformers of Indole···Pyridine Dimer at Various Levels of Theory[a]

	M05-2X/aVDZ		M06-2X/cc-pVDZ		M06-2X/aVDZ	MP2/cc-pVDZ		MP2/aVDZ
	ΔE_e	ΔE_0	ΔE_e	ΔE_0	ΔE_e	ΔE_e	ΔE_0	ΔE_e
HB3	−7.44	−6.48	−7.55	−5.94	−7.37	−7.45	−6.52	−8.70
syn-PD4	−4.61	−4.13	−5.29	−4.21	−6.47	−4.46	−4.08	−8.39
anti-PD3	−2.89	−2.65	−4.97	−3.73	−4.99	−2.90	−2.70	−6.67
T5	−3.82	−2.90	−3.68	−3.26	−3.55	−3.40	−2.97	−5.06

[a] ΔE_e: BSSE corrected binding energy, ΔE_0: BSSE + ZPE corrected binding energy.

Table 3. Geometrical Parameters of Four Conformers of Indole···Pyridine Dimer Calculated at MP2/aug-cc-pVDZ Level of Theory[a]

	HB3	syn-PD4	anti-PD3	T5
$d_{H\cdots N}$ (Å)	1.950	2.970		
$d_{N\cdots N}$ (Å)	2.880	3.170		
Δr_{N-H} (Å)	0.015	0.002		
<N−H−N	149°	92°		
$<C_6C_1N_{16}H_{13}$[b]	−7°	12.6°	−1.71°	
interplanar distance (Å)		3.10	3.11	
$<C_1N_{16}N_{22}C_{17}$[b]	−54°			
$d_{C-H\cdots N}$ (Å)	2.72			2.53
$d_{C-H\cdots\pi}$ (Å)	3.28			
$d_{N-H\cdots\pi}$ (Å)				2.14
ν_{N-H} (cm^{-1})	3246	3505	3523	3528

[a] Frequencies of the four conformers calculated at MP2/cc-pVDZ level of theory are also provided here. [b] For atom numbering of the dimer, see Figure 8a.

the other C−H bonds in the pyridine ring is 1.093 Å. Thus, the indole and pyridine rings in this conformer are not oriented exactly perpendicular to each other through the N−H···N hydrogen bond, but they are bent to each other forming a unique V-shaped herringbone structure. The angle between the two rings, which is described by the dihedral angle $C_1N_{16}N_{22}C_{17}$ (see Figure 8a) and termed as wagging angle is −54°. A similar kind of V-shaped geometry has also been reported for the phenol dimer from various experiments and theoretical calculations.[39−45] In the case of the phenol dimer, there is a strong O−H···O hydrogen bond with a H···O distance of 1.92 Å, O···O distance of 2.88 Å, and the angle between the two phenyl rings (wagging angle) is −69.6°.[41] Very recently, Kim and co-workers have performed extensive calculations for the phenol dimer at various levels of theory.[45] They have reported that the V-shaped structure of the phenol dimer is determined by hydrogen bonding as well as CH···π and $\pi\cdots\pi$ dispersion interactions.

There is a striking difference in the geometry of the two parallel-displaced (PD) π-stacked conformers of the dimer. The syn-PD4 stacked conformer has both indole N−H group and pyridine nitrogen atom in the same side and form weak N−H···N hydrogen bond with H···N distance of 2.97 Å. Due to this hydrogen bonding, the hydrogen atom of NH group of indole goes out of plane to significant extent to point toward the pyridine nitrogen atom. On the other hand, the anti-PD3 stacked dimer has indole N−H group and pyridine nitrogen atom in the opposite side without having any possibility of hydrogen bond formation. The planarity of the N−H group of indole is described by the dihedral angle $<C_6C_1N_{16}H_{13}$, which is 0°, 12.6°, and −1.71° for bare indole, syn-PD4 stacked dimer, and anti-PD3 stacked dimer, respectively. The strongly hydrogen bonded conformer of the dimer also shows nonplanarity of the N−H group by −7° due to the V-shaped geometry. This clearly explains the formation of N−H···N hydrogen bond in case of the syn-PD4 stacked dimer, where the center to center distance between two monomer units is 3.10 Å, which is standard for parallel-displaced dimers. The syn-PD stacked dimer also shows small elongation of NH bond length by 0.002 Å. The T-shaped N−H···π bound dimer (T5) possesses N−H···π dispersion interaction as well as C−H···N electrostatic interaction. The N−H···π ($d_{N-H\cdots\pi}$) and C−H···N ($d_{C-H\cdots N}$) distances in the T5 dimer are 2.14 and 2.53 Å, respectively. It has been found that the NH···π hydrogen-bonded conformer (T5) of the dimer is not a stable minimum, as the frequency calculation of this conformer at various levels of theory with different basis sets provide an imaginary frequency. On the contrary, the NH···π hydrogen-bonded structure is reported to be the most stable conformer in the case of indole···benzene dimer studied by both theory and experiment.[35−37] NH···π hydrogen-bonded conformer of indole···pyridine dimer is unstable, probably because aromatic rings with heteroatoms are poor π-hydrogen bond acceptors, as reported by Sherrill and co-workers.[67]

It will be interesting to compare the hydrogen bond strength of the V-shaped conformer (HB3) of the indole···pyridine dimer with few other hydrogen-bonded complexes of indole reported in the literature.[57,68] Table 4 provides the red-shift of N−H stretching, band origin, and Δr_{N-H} of hydrogen-bonded complexes of indole with H_2O, Me_2S, NH_3, and pyridine, as well as proton affinity[69] of the complexing bases. It is clearly observed that there is a nice correlation of N−H stretching red-shift with Δr_{N-H} in the complex and proton affinity of the acceptors. Proton affinity of both NH_3 and pyridine is much higher than that of H_2O, and Δr_{N-H} is more than double in indole···NH_3 and indole···pyridine complexes compared to that in the indole···H_2O cluster. Red-shift in the N−H stretching frequency in these three complexes is consistent with these data. Actually, the indole···NH_3 cluster is very much suitable to compare with the indole···pyridine dimer in terms of hydrogen bond strength due to the presence of the N−H···N bond in both cases. We have performed geometry optimization and frequency calculation of indole···NH_3 complex at MP2/aug-cc-pVDZ and MP2/cc-pVDZ levels, respectively. Both the indole···pyridine and indole···NH_3 complexes indeed show similar Δr_{N-H} (0.015 Å) and red-shift (more than 250 cm^{-1}) in the N−H stretching frequency. In the case of indole···NH_3 cluster, experimental N−H stretching frequency is not available;

Table 4. Shift in the N−H Stretching Frequencies ($\Delta\nu_{N-H}$) and Band Origin (ΔE_{BO}) for Various Complexes of Indole, and Proton Affinity of Hydrogen Bond Acceptors

		indole complexes		
hydrogen bond acceptors	proton affinity[a] (kcal/mol)	Δr_{N-H} (Å)	$\Delta\nu_{N-H}$ (cm^{-1})	ΔE_{BO} (cm^{-1})
H_2O[b]	166.5	0.007	−89	−132
Me_2S[b]	198.6	0.012	−158	−170
NH_3	204.2	0.015[c]	(−321)	−227[d]
pyridine	219.6	0.015	−257 (−280)	−271

[a] Ref 69. [b] Ref 68. [c] The value calculated in this work at MP2/aVDZ level. The values in the parentheses are theoretical $\Delta\nu_{N-H}$ at MP2/cc-pVDZ level. In the case of the indole···NH_3 complex, experimental $\Delta\nu_{N-H}$ is not available. [d] Refs 53 and 69.

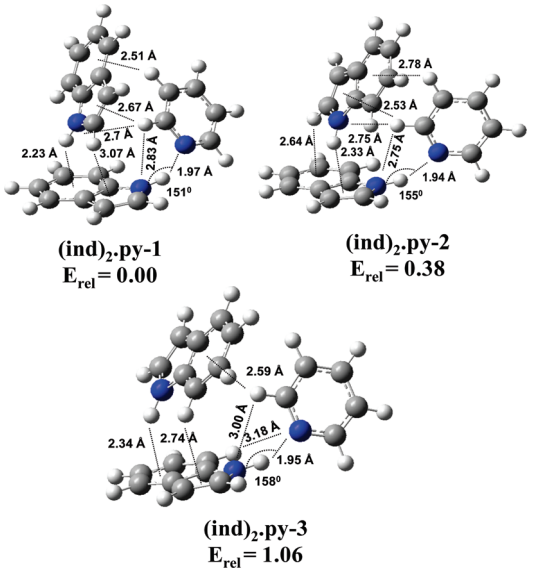

Figure 9. M05-2X/6-311++G** optimized structures of three stable conformers of (indole)$_2$···pyridine trimer. E_{rel} is the ZPE corrected relative energy of the conformers in kcal/mol.

thus, only theoretical value computed by us has been provided. There is also a linear relationship between band origin shift of indole···solvent complexes with proton affinity of the solvents.[53,69,70] It is interesting to note that the band origin shift in the V-shaped indole···pyridine dimer (HB3) is comparable to that of the indole···NH_3 complex. Proton affinity values of NH_3 and pyridine are 204 and 219.6 kcal/mol, respectively,[69] and band origin shifts of the indole···NH_3 complex and indole···pyridine V-shaped dimer are −227 and −271 cm^{-1}, respectively.[53,69] Thus, the assignment of the species B in the R2PI spectrum recorded in the dimer mass channel as V-shaped indole···pyridine dimer (HB3) is strongly confirmed.

3.5.2. Structures of (Indole)$_2$···Pyridine trimer. Initial geometry optimization of various possible conformers of (indole)$_2$···pyridine trimer have been performed at the M05-2X/6-31+G* level. Three low energy structures of the trimer obtained from the M05-2X/6-31+G* level of calculation were further optimized with higher basis sets at M05-2X level as well as M06-2X/cc-pVDZ level. Figure 9 shows the structures of the three conformers of the trimer optimized at the M05-2X/6-311++G** level. All three conformers have cyclic structures with little variation in the orientation of the three monomer units. These three structures are named as (ind)$_2$·py-1, (ind)$_2$·py-2, and (ind)$_2$·py-3. Similar kinds of cyclic structures have been reported for naphthalene trimer, phenol trimer, and a few *N*-heteroaromatic systems like pyridine trimer, pyrazine trimer, and so on.[40,71,72] All three structures of (indole)$_2$···pyridine trimer studied here are stabilized by strong N−H···N and weak C−H···N electrostatic interactions, as well as multiple dispersion interactions between two indole rings and pyridine with each of the indole rings. In the (ind)$_2$·py-1 structure, two indole rings are interacting with each other through N−H···π and C−H···π interactions, where a N−H group and one C−H group of the indole ring are forming hydrogen bonds with the π-clouds of phenyl and pyrrole groups of the other indole ring, respectively. On the other hand, two C−H groups of pyridine are forming two C−H···π hydrogen bonds with pyrrole and phenyl groups of one of the indole rings. One of the π-hydrogen bound C−H groups of pyridine also forms weak C−H···N hydrogen bonds with the nitrogen atoms of both of the indole rings. In the case of the (ind)$_2$·py-2 structure, similar types of electrostatic and dispersion interactions are present, except two indole rings that are interacting with each other slightly differently. Here, the N−H group and one C−H group of indole are interacting with the π-clouds of pyrrole and phenyl groups of the other indole ring, respectively. In the case of (ind)$_2$·py-3 structure, two indole rings are interacting with each other in a similar fashion, like the (ind)$_2$·py-1 structure, but interaction between pyridine and the indole rings is different compared to that for the other two trimer structures. There is only one C−H···π interaction between pyridine and the indole rings in the (ind)$_2$·py-3 structure.

BSSE and zero point energy (ZPE) corrected binding energies and ZPE corrected relative energies of the three cyclic structures of the trimer calculated at various levels of theory are presented in Table 5. Comparison of binding energies as well as relative energies at different levels of theory show that (ind)$_2$·py-1 is the most stable trimer structure. Table 6 provides theoretical N−H stretching frequencies and Δr_{N-H} (change in N−H bond lengths in complex formation) of the three structures of the trimer. Theoretical N−H stretching frequencies of the trimer, presented in Table 6, have been obtained from M05-2X/6-311++G** level of calculation, and the frequencies are corrected with a scaling factor of 0.9388. The strength of the hydrogen bond is generally reflected in the red-shift in the N−H stretching frequency as well as the extent of the lengthening of the N−H bond. The result shows that the experimental red-shift in the σ-bond (N−H···N) N−H stretching frequency of the trimer is 245 cm^{-1} and the lengthening of the corresponding N−H bond length in the three trimeric structures is 0.016−0.017 Å. On the other hand, the π-bound (N−H···π) N−H stretching

Table 5. Relative Energies (kcal/mol), ZPE, and BSSE Corrected Binding Energies (kcal/mol) of Three Conformers of $(Indole)_2\cdots$Pyridine Trimer Calculated at Various Levels of Theory[a]

	M05-2X/6-311++G**			M05-2X/cc-pVDZ			M06-2X/cc-pVDZ		
	ΔE_e	ΔE_0	E_{rel}	ΔE_e	ΔE_0	E_{rel}	ΔE_e	ΔE_0	E_{rel}
$(Ind)_2$ ·Py-1	−19.41	−17.63	0.00	−19.00	−17.19	0.00	−20.67	−18.20	0.00
$(Ind)_2$ ·Py-2	−18.96	−17.24	0.38	−18.42	−16.63	0.55	−19.76	−17.51	0.70
$(Ind)_2$ ·Py-3	−18.22	−16.57	1.06	−17.87	−16.27	0.91	−18.65	−16.49	1.71

[a] ΔE_e: BSSE corrected binding energy; ΔE_0: BSSE + ZPE corrected binding energy; E_{rel}: ZPE corrected relative energy of the conformers with respect to the most stable conformer.

Table 6. N−H···N and N−H···π Bound N−H Stretching Frequencies and Change in N−H Bond Lengths of Three Conformers of the Trimer Calculated at the M05-2X/6-311++G Level of Theory[a]**

	ν_{N-H} (N−H···N; cm^{-1})	ν_{N-H} (N−H···π; cm^{-1})	Δr_{N-H} (N−H···N; Å)	Δr_{N-H} (N−H···π; Å)
$(ind)_2$·py-1	3270 (734)	3452 (304)	0.016	0.006
$(ind)_2$·py-2	3231 (939)	3420 (373)	0.017	0.008
$(ind)_2$·py-3	3259 (822)	3440 (273)	0.016	0.007

[a] Intensity in km/mol is given in parentheses. Frequencies have been scaled by a factor of 0.9388.

Table 7. Interaction Energies (kcal/mol) in Various Conformers of the Dimer and the most Stable Structure of the Trimer, Calculated at M05-2X/aug-cc-pVDZ and M05-2X/cc-pVDZ Levels of Theory, Respectively

	ΔE_{ele}	ΔE_{ex}	ΔE_{rep}	ΔE_{pol}	ΔE_{disp}	ΔE_{tot}
HB3-dimer	−11.10	−6.47	21.57	−3.81	−7.77	−7.57
PD4-dimer	−4.97	−4.76	21.26	−1.60	−14.71	−4.78
PD3-dimer	−2.68	−4.19	19.38	−1.50	−13.89	−2.88
T5-dimer	−3.63	−2.31	11.70	−0.90	−8.67	−3.82
$(ind)_2$·Py-1 trimer	−24.22	−15.55	58.63	−8.44	−30.08	−19.66

frequency of the trimer is red-shifted by 115 cm^{-1}, and the increase in the corresponding N−H bond length in the three structures of the trimer is 0.006−0.008 Å. It has been found that the theoretical N−H stretching frequencies (N−H···N as well N−H···π hydrogen bonded) of the three cyclic structures of the trimer corroborate in a similar fashion with the experimental N−H stretching frequencies of the trimer observed in the experiment. But, from an energetic point of view, the $(ind)_2$·py-1 structure is the global minimum and it also has maximum binding energy. Thus, the observed trimer is assigned to have $(ind)_2$·py-1 structure.

3.5.3. Energy Decomposition Analysis (EDA) of the Dimer and the Trimer. For quantitative determination of the various contributions to the stabilization of different conformers of the dimer and the trimer, localized molecular orbital-energy decomposition analysis (LMO-EDA) procedure introduced by Su and Li is used.[73] In the LMO-EDA method, total interaction energy (ΔE_{total}) of the complex is decomposed into electrostatic (ΔE_{ele}), exchange (ΔE_{ex}), repulsion (ΔE_{rep}), polarization (ΔE_{pol}), and dispersion (ΔE_{disp}) components. Table 7 shows the different contributions of the interaction energy of various conformers of the dimer as well as the most stable structure of the trimer $(ind)_2$·py-1. EDA calculations of the dimer and the trimer have been performed at M05-2X/aug-cc-pVDZ and M05-2X/cc-pVDZ levels, respectively. The result clearly shows that dispersion interaction plays a significant role in the stabilization of the electrostatic dominated dimer HB3. The electrostatic component of the total interaction energy of the HB3 dimer is −11.1 kcal/mol, whereas the dispersion component is −7.77 kcal/mol. In the case of the dispersion dominated π-stacked dimers, syn-PD4 has indeed more electrostatic contribution in the total interaction energy than the anti-PD3 conformer. This favors the weak N−H···N hydrogen bonding interaction in the case of syn-PD4. It is also obvious from the calculation that dispersion interaction is the dominating force in the stabilization of the NH···π hydrogen-bonded T5 conformer of the dimer.

EDA analysis of $(ind)_2$·py-1 structure of the trimer shows that the contribution of the dispersion interaction is more compared to the electrostatic interaction in stabilization of the trimer geometry. The electrostatic component of the total interaction energy of the trimer is −24.22 kcal/mol, whereas the dispersion component is −30.08 kcal/mol. This supports the premise that the trimer geometry is comprised of multiple dispersion interactions, that is, N−H···π and few C−H···π interactions, in addition to strong N−H···N and weak C−H···N electrostatic interactions.

3.5.4. TDDFT Analysis of the Dimer and the Trimer. Single-point TDDFT calculation at M05-2X/cc-pVDZ level has been performed to compute $S_0 \rightarrow S_1$ transition frequencies of the dimer and the trimer. It is known that the absolute value of $S_0 \rightarrow S_1$ transition energy obtained from TDDFT calculation is quite far away from the experimental vertical excitation energy. But the theoretical relative $S_0 \rightarrow S_1$ origin frequencies are very often useful to assign different species or conformers present in the experiment. The computed transition frequencies of the HB3 conformer of the dimer and the most stable conformer of the trimer, scaled to the experimental band origin of indole, are 300.62 and 292.21 nm, respectively. The corresponding experimental transition frequencies of the dimer and trimer are 285.95 and 284.38 nm, respectively. Thus, TDDFT calculation supports the experimental observation that the electronic origin band of the dimer in comparison with the trimer is more red-shifted from the origin band of the monomer. Comparison of TDDFT calculated and experimental $S_0 \rightarrow S_1$ transition frequencies of different conformers of isolated molecules as well as complexes has been reported by several authors in the literature.[74,75]

4. CONCLUSIONS

In summary, we have studied the structures of indole···pyridine dimer and (indole)$_2$···pyridine trimer in a supersonic jet using one-color R2PI, IR-UV double resonance spectroscopic techniques, and quantum chemistry calculations. R2PI spectra of the dimer and trimer have been measured by electronic excitation of the indole moiety. The electronic origin bands of the dimer and the trimer are red-shifted from the 0_0^0 band for the $S_0 \rightarrow S_1$ transition of the indole monomer by 76 and 271 cm^{-1}, respectively. R2PI spectrum obtained in the dimer mass channel exhibits extensive fragmentation from the trimer. RIDIR spectra combined with IR-UV hole-burning spectra confirm the presence of only one conformer in the experiment for both of the dimer and the trimer. RIDIR spectra show that there is a large red-shift (−257 cm^{-1}) in the N−H stretching frequencies of the dimer compared to that in the indole monomer. MP2, as well as DFT/M05-2X, and DFT/M06-2X calculations predict that the observed dimer has V-shaped structure stabilized by strong N−H···N and weak C−H···N hydrogen bonding interactions, as well as CH···π and π···π dispersion interactions. RIDIR spectra, combined with DFT/M05-2X and DFT/M06-2X calculations, confirm that the observed trimer has a cyclic structure with N−H···N, N−H···π, C−H···N, and C−H···π interactions. In the future it will be possible to shed further light on the structures of the dimer and trimer by using rotational coherence spectroscopy as well as rotationally resolved electronic spectroscopy.

■ ASSOCIATED CONTENT

Ⓢ Supporting Information. R2PI spectrum in (indole)$_2$···pyridine···H_2O mass channel, RIDIR spectra by probing all three electronic bands in the region of the dimer, IR-UV hole-burning spectra by probing the vibrational band of the trimer at 3309 cm^{-1}, initial and MP2/6-31+G* optimized structures of all the conformers of indole···pyridine dimer, intermolecular vibrational frequencies of the trimer calculated in the ground electronic state, and ZPE corrected relative energies of various conformer of the dimer. This material is available free of charge via the Internet at http://pubs.acs.org.

■ AUTHOR INFORMATION

Corresponding Author

*Phone: 91-20-2590-8078. Fax: 91-20-2589-9790. E-mail: a.das@iiserpune.ac.in.

■ ACKNOWLEDGMENT

The authors gratefully acknowledge the financial support received from the Indian Institute of Science Education and Research (IISER) Pune to carry out the research. S.K. thanks CSIR for the research fellowship; P.B. and I.K. thank IISER Pune for their fellowships. Research support from IISER Pune supercomputer facility is also acknowledged. Partial financial support from DST nanoscience unit of IISER (Project No. SR/NM/Z-3/2007) is also acknowledged. The authors wish to acknowledge the reviewers for their valuable comments. The authors are thankful to Dr. Prasenjit Pandey, Research Associate, Indian Association for the Cultivation of Science, Kolkata, India, for fruitful discussions on Energy Decomposition Analysis of the dimer and trimer studied here.

■ REFERENCES

(1) Saenger, W. *Principles of Nucleic Acid Structure*; Springer-Verlag: New York, 1984.
(2) Burley, S. K.; Petsko, G. A. *Science* **1985**, *229*, 23.
(3) Meyer, E. A.; Castellano, R. K.; Diederich, F. *Angew. Chem., Int. Ed.* **2003**, *42*, 1210.
(4) Desiraju, G. R. *Angew. Chem., Int. Ed.* **1995**, *34*, 2311.
(5) Hong, B. H.; Bae, S. C.; Lee, C.-W.; Jeong, S.; Kim, K. S. *Science* **2001**, *294*, 348.
(6) Lehn, J.-M. *Supramolecular Chemistry: Concepts and Perspectives*; VCH: New York, 1995.
(7) Steed, J. W.; Atwood, J. L. *Supramolecular Chemistry: A Concise Introduction*; Wiley: New York, 2000.
(8) Hunter, C. A. *Chem. Soc. Rev.* **1994**, *23*, 101.
(9) Hoeben, F. J. M.; Jonkheijm, P.; Meijer, E. W.; Schenning, A. P. H. *Chem. Rev.* **2005**, *105*, 1491.
(10) Singh, N. J.; Lee, H. M.; Suh, S. B.; Kim, K. S. *Supramol. Chem.* **2007**, *19*, 321.
(11) Sygula, A.; Fronczek, F. R.; Sygula, R.; Rabideau, P. W.; Olmstead, M. M. *J. Am. Chem. Soc.* **2007**, *129*, 3842.
(12) Shieh, H. − S.; Berman, H. M.; Dabrow, M.; Neidle, S. *Nucleic Acids Res.* **1980**, *8*, 85.
(13) Henson, B. F.; Hartland, G. V.; Venturo, V.; Hertz, R. A.; Felker, P. M. *Chem. Phys. Lett.* **1991**, *176*, 91.
(14) Henson, B. F.; Hartland, G. V.; Venturo, V.; Hertz, R. A.; Felker, P. M. *J. Chem. Phys.* **1992**, *97*, 2189.
(15) Arunan, E.; Gutowsky, H. S. *J. Chem. Phys.* **1993**, *98*, 4294.
(16) Schaeffer, M. W.; Maxton, P. M.; Felker, P. M. *J. Chem. Phys.* **1994**, *101*, 8391.
(17) Erlekam, U.; Frankowski, M.; Meijer, G.; von Helden, G. *J. Chem. Phys.* **2006**, *124*, 171101.
(18) Erlekam, U.; Frankowski, M.; von Helden, G.; Meijer, G. *Phys. Chem. Chem. Phys.* **2007**, *9*, 3786.
(19) Hobza, P.; Selzle, H. L.; Schlag, E. W. *J. Am. Chem. Soc.* **1994**, *116*, 3500.
(20) Tsuzuki, S.; Honda, K.; Uchimaru, T.; Mikami, M.; Tanabe, K. *J. Am. Chem. Soc.* **2002**, *124*, 3842.
(21) Sinnokrot, M. O.; Valeev, E. F.; Sherrill, C. D. *J. Am. Chem. Soc.* **2002**, *124*, 10887.
(22) Sinnokrot, M. O.; Sherrill, C. D. *J. Phys. Chem. A* **2004**, *108*, 10200.
(23) Sinnokrot, M. O.; Sherrill, C. D. *J. Phys. Chem. A* **2006**, *110*, 10656.
(24) Podeszwa, R.; Bukowski, R.; Szalewicz, K. *J. Phys. Chem. A* **2006**, *110*, 10345.
(25) DiStasio, R. A.; Von Helden, G.; Steele, R. P.; Head-Gordon, M. *Chem. Phys. Lett.* **2007**, *437*, 277.
(26) Janowski, T.; Pulay, P. *Chem. Phys. Lett.* **2007**, *447*, 27.
(27) Lee, E. C.; Kim, D.; Jurecka, P.; Tarakeswar, P.; Hobza, P.; Kim., K. S. *J. Phys. Chem. A* **2007**, *111*, 3446.
(28) Pitonak, M.; Neogrady, P.; ORezac, J.; Jurecka, P.; Urban, M.; Hobza, P. *J. Chem. Theory Comput.* **2008**, *4*, 1829.
(29) Grafenstein, J.; Cremer, D. *J. Chem. Phys.* **2009**, *130*, 124105.
(30) Mons, M.; Dimicoli, I.; Tardivel, B.; Piuzzi, F.; Brenner, V.; Millie, P. *Phys. Chem. Chem. Phys.* **2002**, *4*, 571.
(31) Vaupel, S.; Brutschy, B.; Tarakeshwar, P.; Kim, K. S. *J. Am. Chem. Soc.* **2006**, *128*, 5416.
(32) Matsumoto, Y.; Honma, K. *J. Chem. Phys.* **2007**, *127*, 184310.
(33) Dauster, I.; Rice, C. A.; Zielke, P.; Suhm, M. A. *Phys. Chem. Chem. Phys.* **2008**, *10*, 2827.
(34) Ottiger, P.; Pfaffen, C.; Leist, R.; Leutwyler, S.; Bachorz, R. A.; Klopper, W. *J. Phys. Chem. B* **2009**, *113*, 2937.
(35) Braun, J. E.; Grebner, Th.L.; Neusser, H. J. *J. Phys. Chem. A* **1998**, *102*, 3273.
(36) Braun, J. E.; Neusser, H. J.; Hobza, P. *J. Phys. Chem. A* **2003**, *107*, 3918.
(37) Geng, Y.; Takatani, T.; Hohenstein, E. G.; Sherrill, C. D. *J. Phys. Chem. A* **2010**, *114*, 3576.

(38) Jurecka, P.; Sponer, J.; Cerny, J.; Hobza, P. *Phys. Chem. Chem. Phys.* **2006**, *8*, 1985.
(39) Felker, P. M. *J. Phys. Chem.* **1992**, *96*, 7844.
(40) Ebata, T.; Watanabe, T.; Mikami, N. *J. Phys. Chem.* **1995**, *99*, 5761.
(41) Weichert, A.; Reihn, C.; Brutschy, B. *J. Phys. Chem. A* **2001**, *105*, 5679.
(42) Hobza, P.; Riehn, C.; Weichert, A.; Brutschy, B. *Chem. Phys.* **2002**, *283*, 331.
(43) Kolar, M.; Hobza, P. *J. Phys. Chem. A* **2007**, *111*, 5851.
(44) Brause, R.; Santa, M.; Schmitt, M.; Kleinermanns, K. *Chem. Phys. Chem.* **2007**, *8*, 1394.
(45) Kolaski, M.; Kumar, A.; Singh, N. J.; Kim, K. S. *Phys. Chem. Chem. Phys.* **2010**, *12*, 6278.
(46) Sanders, J. M. *J. Phys. Chem. A* **2010**, *114*, 9205.
(47) Cilento, G.; Tededchi, P. *J. Biol. Chem.* **1961**, *236*, 907.
(48) Wiley, W. C.; McLaren, I. H. *Rev. Sci. Instrum.* **1955**, *26*, 1150.
(49) Boys, S. F.; Bernardi, F. *Mol. Phys.* **1970**, *19*, 553.
(50) Schmidt, M. W.; Baldridge, K. K.; Boatz, J. A.; Elbert, S. T.; Gordon, M. S.; Jesnsen, J. H.; Koseki, S.; Matsunaga, N.; Nguyen, K. A.; Su, S. J.; Windus, T. L.; Dupuis, M.; Montgomery, J. A. *J. Comput. Chem.* **1993**, *14*, 1347.
(51) Frisch, M. J.; Trucks, G. W.; Schlegel, H. B.; et al. *Gaussian 03*, Revision E.01; Gaussian, Inc.: Wallingford, CT, 2004.
(52) Bylaska, E. J.; de Jong, W. A.; Govind, N.; et al. *NWChem*, A Computational Chemistry Package for Parallel Computers, Version 5.1.1; Pacific Northwest National Laboratory: Richland, WA, 2008.
(53) Hager, J. W.; Demmer, D. R.; Wallace, S. C. *J. Phys. Chem.* **1987**, *91*, 1375.
(54) Sobolewski, A. L.; Domcke, W. *J. Phys. Chem. A* **2007**, *111*, 11725.
(55) Hager, J. W.; Wallace, S. C. *J. Phys. Chem.* **1984**, *88*, 5513.
(56) Villa, E.; Amirav, A.; Lim, E. C. *J. Chem. Phys.* **1988**, *92*, 5393.
(57) Carney, J. R.; Zwier, T. S. *J. Phys. Chem. A* **1999**, *103*, 9943.
(58) Biswal, H. S.; Wategaonkar, S. *J. Phys. Chem. A* **2010**, *114*, 5947.
(59) Maity, S.; Patwari, G. N. *J. Phys. Chem. A* **2010**, *114*, 8337.
(60) Patwari, G. N.; Ebata, T.; Mikami, N. *J. Chem. Phys.* **2002**, *116*, 6056.
(61) Nibu, Y.; Marui, R.; Shimada, H. *J. Phys. Chem. A* **2006**, *110*, 12597.
(62) Stein, S. E. IR Spectra. In *NIST Chemistry WebBook*; Mallard, W. G., Linstrom, P. J., Eds.; National Institute of Standards and Technology: Gaithersburg, MD, 2000; NIST Standard Reference Database Number 69; pyridine (http://webbook.nist.gov).
(63) Sickle, K. V.; Culberson, L. M.; Holzmacher, J. L.; Cafiero, M. *Int. J. Quantum Chem.* **2007**, *107*, 1523.
(64) Geng, Y.; Takatani, T.; Hohenstein, E. G.; Sherrill, C. D. *J. Phys. Chem. A* **2010**, *114*, 3576.
(65) Zhao, Y.; Truhlar, D. G. *Acc. Chem. Res.* **2008**, *41*, 157.
(66) Sponer, J.; Riley, K. E.; Hobza, P. *Phys. Chem. Chem. Phys.* **2008**, *10*, 2595.
(67) Hohenstein, E. G.; Sherrill, C. D. *J. Phys. Chem. A* **2009**, *113*, 878.
(68) Biswal, H. S.; Wategaonkar, S. *J. Phys. Chem. A* **2009**, *113*, 12763.
(69) Hunter, E. P.; Lias, S. G. *J. Phys. Chem. Ref. Data* **1998**, *27*, 413.
(70) Tubergen, M. J.; Levy, D. H. *J. Phys. Chem.* **1991**, *95*, 2175.
(71) Benharash, P.; Gleason, M. J.; Felker, P. M. *J. Phys. Chem. A* **1999**, *103*, 1442.
(72) Mishra, B. K.; Sathyamurthy, N. *J. Phys. Chem. A* **2010**, *114*, 9606.
(73) Su, P.; Li, H. *J. Chem. Phys.* **2009**, *131*, 014102.
(74) Leist, R.; Frey, J. A.; Ottiger, P.; Frey, H.-M.; Leutwyler, S.; Bachorz, R. A.; Klopper, W. *Angew. Chem., Int. Ed.* **2007**, *46*, 7449.
(75) James, W. H., III; Muller, C. W.; Buchanan, E. G.; Nix, M. G. D.; Guo, L.; Roskop, L.; Gordon, M. S.; Slipchenko, L. V.; Gellman, S. H.; Zwier, T. S. *J. Am. Chem. Soc.* **2009**, *131*, 14243.